

Geophysical Research Letters®

RESEARCH LETTER

10.1029/2022GL101901

Key Points:

- Precipitation d-excess and $\Delta^{17}\text{O}$ are affected by a combination of oceanic moisture source (OMS) conditions and other regional/local factors
- OMS temperature and humidity together explain 41% of the variability in precipitation d-excess in low- and mid-latitudes
- The theoretically contrasting sensitivity between d-excess and $\Delta^{17}\text{O}$ to OMS temperature is validated

Supporting Information:

Supporting Information may be found in the online version of this article.

Correspondence to:

Z. Xia,
zhyxia@hotmail.com

Citation:

Xia, Z. (2023). Quantifying the fingerprint of oceanic moisture source conditions in deuterium and ^{17}O excess parameters of precipitation. *Geophysical Research Letters*, 50, e2022GL101901. <https://doi.org/10.1029/2022GL101901>


Received 27 OCT 2022

Accepted 15 FEB 2023

© 2023. The Authors.

This is an open access article under the terms of the [Creative Commons Attribution License](https://creativecommons.org/licenses/by/4.0/), which permits use, distribution and reproduction in any medium, provided the original work is properly cited.

Quantifying the Fingerprint of Oceanic Moisture Source Conditions in Deuterium and ^{17}O Excess Parameters of Precipitation

Zhengyu Xia¹ 

¹Key Laboratory of Geographical Processes and Ecological Security in Changbai Mountains, Ministry of Education, School of Geographical Sciences, Northeast Normal University, Changchun, China

Abstract The deuterium excess (d-excess) and more recently developed ^{17}O excess ($\Delta^{17}\text{O}$) of precipitation are isotopic tracers that are sensitive to oceanic moisture source (OMS) conditions. However, other regional and local processes also affect precipitation d-excess and $\Delta^{17}\text{O}$ and may modify or overprint their OMS signals. Here, I leverage the new atmospheric moisture flow data set to diagnose the OMS regions and conditions globally and show that OMS temperature and relative humidity together explain 41% of the variability in monthly mean precipitation d-excess in low- and mid-latitudes. Based on a few sites currently having paired d-excess and $\Delta^{17}\text{O}$ data, I also show that the contrasting sensitivity between d-excess and $\Delta^{17}\text{O}$ to OMS temperature, which is initially predicted by theory, is distinguishable from precipitation observations under annual mean conditions. This study contributes to disentangling the complex controls on precipitation d-excess and $\Delta^{17}\text{O}$ by quantifying the crucial role of OMS dynamics.

Plain Language Summary Stable isotopes of water molecules are process tracers of the water cycle. The “excess” quantities of deuterium and ^{17}O in precipitation are second-order isotopic parameters that are sensitive to moisture source conditions over oceans. However, these isotopic “excess” values measured in precipitation are also affected by other factors, such as continental moisture recycling and local condensation or evaporation of raindrops. Here, a new atmospheric moisture flow data set is used to diagnose oceanic moisture source (OMS) regions and conditions across the globe. In this way, the OMS fingerprint in terrestrial precipitation sites is directly quantified. The analysis indicates that OMS temperature and relative humidity together explain 41% of the variability in precipitation deuterium excess in low- and mid-latitude sites, meaning that most of the variability might be attributed to other processes. While ^{17}O excess data are currently limited to a few sites, the analysis also clearly distinguishes that precipitation ^{17}O excess is insensitive but deuterium excess is sensitive to OMS temperature under annual mean conditions. This finding validates an earlier theory-based prediction. The quantitative appraisal of the OMS effect presented in this study assists in disentangling the complex controls of water isotope tracers.

1. Introduction

The stable isotopes of precipitation are powerful tracers of the water cycle (Gat, 1996). The second-order isotopic parameter deuterium excess (d-excess), calculated as $\delta^2\text{H} - 8 \times \delta^{18}\text{O}$ (δ -notation uses the unit ‰), was conceived to track kinetic fractionation and is highly sensitive to conditions during the evaporation of ocean surface water (Dansgaard, 1964). For a long time, the d-excess of precipitation has been viewed as a fingerprint of oceanic moisture source (OMS) conditions (Armengaud et al., 1998; Johnsen et al., 1989; Merlivat & Jouzel, 1979). The signals of d-excess preserved in ice cores or ancient groundwater were used as a proxy to reconstruct past OMS conditions (Jouzel et al., 1982; Rozanski, 1985; Vimeux et al., 1999). The excess abundance of ^{17}O over ^{18}O , now denoted as $\Delta^{17}\text{O}$ (Aron et al., 2021), is an isotopic parameter recently developed for the same purpose as d-excess (as another potential OMS tracer) and has been increasingly measured in precipitation or other natural waters as well as in polar ice cores (Bershaw et al., 2020; Landais et al., 2008; Li et al., 2015; Luz & Barkan, 2010). It is specifically calculated as follows:

$$\Delta^{17}\text{O} \text{ (per meg)} = (\delta^{17}\text{O} - 0.528 \times \delta^{18}\text{O}) \times 1,000 \text{ (Barkan \& Luz, 2007)} \quad (1)$$

with

$$\delta'(\text{‰}) = \ln(\delta/1,000 + 1) \times 1,000 \quad (2)$$

Despite their high sensitivities to OMS conditions, precipitation d-excess and $\Delta^{17}\text{O}$ are also affected by other regional and local processes that may modify or overprint their OMS signals. For example, high precipitation d-excess values were found downwind of large lakes, forests, or irrigated farmlands, and indicate upwind moisture recycling via evaporation (Gat et al., 1994; Gat & Matsui, 1991; Taupin et al., 2000), while low precipitation d-excess values were found in dry areas or periods and indicate that sub-cloud re-evaporation of falling raindrops has occurred (Pang et al., 2011; Putman et al., 2019). By definition, these kinetic fractionation-related processes similarly affect $\Delta^{17}\text{O}$ (Aron et al., 2021; Bershaw et al., 2020; Li et al., 2015). Disentangling the contributions of multiple fractionation processes to the variability of d-excess and $\Delta^{17}\text{O}$ in precipitation is essential for an unambiguous interpretation of isotopic tracers in both modern and paleo-environments (Risi et al., 2013; Xia et al., 2022).

Additionally, when $\Delta^{17}\text{O}$ was first introduced, isotope theory predicted that while d-excess is sensitive to both sea surface temperature (SST) and oceanic relative humidity (RH) at the OMS, $\Delta^{17}\text{O}$ is insensitive to SST and only sensitive to oceanic RH (Angert et al., 2004). This distinction implies that a combination of d-excess and $\Delta^{17}\text{O}$ data may provide complementary information about OMS conditions in ice-core paleoclimate records (Jouzel et al., 2013; Landais et al., 2008). However, direct observational evidence to validate this theory-based prediction or application is sparse (Landais et al., 2012; Uemura et al., 2010), in part due to non-OMS processes that compromise OMS signals in precipitation observations (Li et al., 2015; Schoenemann et al., 2014).

Here, I apply the recently released atmospheric moisture flow data set by Tuinenburg et al. (2020) to diagnose OMS regions and conditions across the globe. Thereby I investigate the specific contribution of OMS dynamics to the variability in precipitation d-excess in low- and mid-latitudes and demonstrate the theoretically contrasting sensitivity between d-excess and $\Delta^{17}\text{O}$ to OMS SST.

2. Data and Methods

2.1. Precipitation Isotope Data Set

The amount-weighted 12 monthly mean d-excess values are calculated at 1.0° grids (if that grid contains ≥ 3 individual monthly measurements) across 60°N – 60°S using data from the Global Network of Isotopes in Precipitation (GNIP) program (IAEA/WMO, 2021). The amount-weighted annual mean d-excess values are calculated for grids that contain complete 12 monthly mean d-excess values.

At present, precipitation $\Delta^{17}\text{O}$ data are available in a few case studies of specific sites. There are 12 sites that have reported precipitation $\Delta^{17}\text{O}$ data for at least 2 yr, with eight sites in Switzerland (Affolter et al., 2015; Leuenberger & Ranjan, 2021) and others in Singapore (He et al., 2021), Okinawa Island (Uechi & Uemura, 2019), Indianapolis in the U.S. (Tian & Wang, 2019), and the Pyrenees in Spain (Giménez et al., 2021). All these sites contain paired d-excess data. Their amount-weighted 12 monthly and annual mean d-excess and $\Delta^{17}\text{O}$ values are either available or calculated here. Arithmetic mean values are used for seven Switzerland sites where precipitation amount data are unavailable (Leuenberger & Ranjan, 2021).

Data screening procedures and uncertainty estimates are described in Text S1 in Supporting Information S1.

2.2. OMS Regions and Conditions

The recently available global atmospheric moisture flow data set of 1.0° spatial resolution generated from the Lagrangian atmospheric moisture tracking model UTrack (forced by ERA5 reanalysis) is used to diagnose OMS regions (Tuinenburg & Staal, 2020; Tuinenburg et al., 2020). This data set provides 12 monthly means of atmospheric moisture flows between all pairs of grid cells globally during 2008–2017. For monthly precipitation at any grid cell of interest, the contribution of evaporation from each cell (either oceanic or terrestrial cell) to that precipitation cell in that month is:

$$s_{ij} = \frac{E_i m_{ij}}{\sum_{i \in \text{globe}} E_i m_{ij}} \quad (3)$$

where s_{ij} is the ratio of precipitation at cell j that sources from evaporation at cell i , E_i is the evaporation flux at cell i , m_{ij} is the fraction of evaporation at cell i that falls as precipitation at cell j (i.e., the atmospheric moisture flow), and Σ symbol denotes the summation of $E_i m_{ij}$ from all evaporation cells globally. The fraction of precipitation at cell j that sources from only ocean grid cells (including large lakes) is $\sum_{i \in \text{ocean}} s_{ij}$ and is termed as OMS ratio here.

The 12 monthly means of gridded SST and oceanic RH (with respect to SST) at 1.0° spatial resolution during 2008–2017 are derived from ERA5 reanalysis (Hersbach et al., 2020) and used to determine OMS conditions. For monthly precipitation at any grid cell of interest, its OMS condition is the SST and oceanic RH averaged over all ocean grid cells weighted by the contribution of evaporation to that precipitation cell in that month like:

$$\overline{sSST}_j = \frac{\sum_{i \in \text{ocean}} s_{ij} SST_i}{\sum_{i \in \text{ocean}} s_{ij}} \quad (4)$$

where \overline{sSST}_j denotes the flux-weighted mean SST at the OMS of precipitation cell j (i.e., OMS SST) and SST_i denotes the SST at evaporation cell i . The same can be written for the flux-weighted mean oceanic RH (i.e., OMS RH). These gridded products of 12 monthly means of OMS SST and RH can be used to calculate the annual means of OMS SST and RH after being weighted by ERA5 precipitation amount.

Importantly, the OMS here only refers to the direct supply of oceanic moisture to the precipitation cell. It does not include the indirect, cascading supply of oceanic moisture, which is described and discussed in Text S2 in Supporting Information S1. To avoid confusion, it should be redundantly termed as direct OMS when necessary, to be distinguished from cascading OMS (Figure S1 in Supporting Information S1).

2.3. Modeling OMS Vapor d-excess and $\Delta^{17}\text{O}$

The OMS SST and RH are converted to OMS vapor d-excess and $\Delta^{17}\text{O}$ using two models. The simple linear regression (SLR) model is based on the empirical relationship between oceanic vapor d-excess/ $\Delta^{17}\text{O}$ and oceanic RH (h_s , in %) in observations as follows:

$$\text{d-excess (‰)} = -0.54 \times h_s + 48.2 \quad (\text{Pfahl \& Sodemann, 2014}) \quad (5)$$

and

$$\Delta^{17}\text{O (per meg)} = -0.74 \times h_s + 65.3 \quad (\text{Uemura et al., 2010}) \quad (6)$$

The SLR model for d-excess has excluded the SST as an independent driver, as argued by Pfahl and Sodemann (2014).

The “closure assumption” (CA) model assumes that oceanic boundary layer moisture is only supplied by oceanic evaporative fluxes (Craig & Gordon, 1965; Merlivat & Jouzel, 1979). It explicitly simulates the isotopic composition of oceanic vapor (δ_{ov}) from Fick's law as follows:

$$\delta_{ov} (\text{‰}) = \frac{(\alpha_{eq})^{-1} \left(\frac{D'}{D} \right)^m (\delta_o + 1,000)}{1 - \left(\frac{h_s}{100} \right) \left[1 - \left(\frac{D'}{D} \right)^m \right]} - 1,000 \quad (7)$$

where α_{eq} is the liquid-vapor equilibrium fractionation factor at SST (>1), D'/D is the diffusivity ratio of water vapor isotopologues, m is the aerodynamic exponent, and δ_o is the isotopic composition of ocean water (assumed as 0‰). The equations of α_{eq} for $^2\text{H}/^1\text{H}$ and $^{18}\text{O}/^{16}\text{O}$ can be found in Majoube (1971). The D'/D is 0.9757 for $^2\text{H}/^1\text{H}$ and 0.9727 for $^{18}\text{O}/^{16}\text{O}$ from Merlivat (1978). For $^{17}\text{O}/^{16}\text{O}$, the values of α_{eq} and D'/D for $^{18}\text{O}/^{16}\text{O}$ are replaced by $(\alpha_{eq})^{0.529}$ and $(D'/D)^{0.518}$ based on the recently determined triple oxygen isotope fractionation exponents (Barkan & Luz, 2005, 2007). The aerodynamic exponent m is ~ 0.25 for open oceans (Gat, 1996; Pfahl & Wernli, 2009). Equation 7 thus predicts OMS vapor d-excess and $\Delta^{17}\text{O}$ from both SST and oceanic RH drivers.

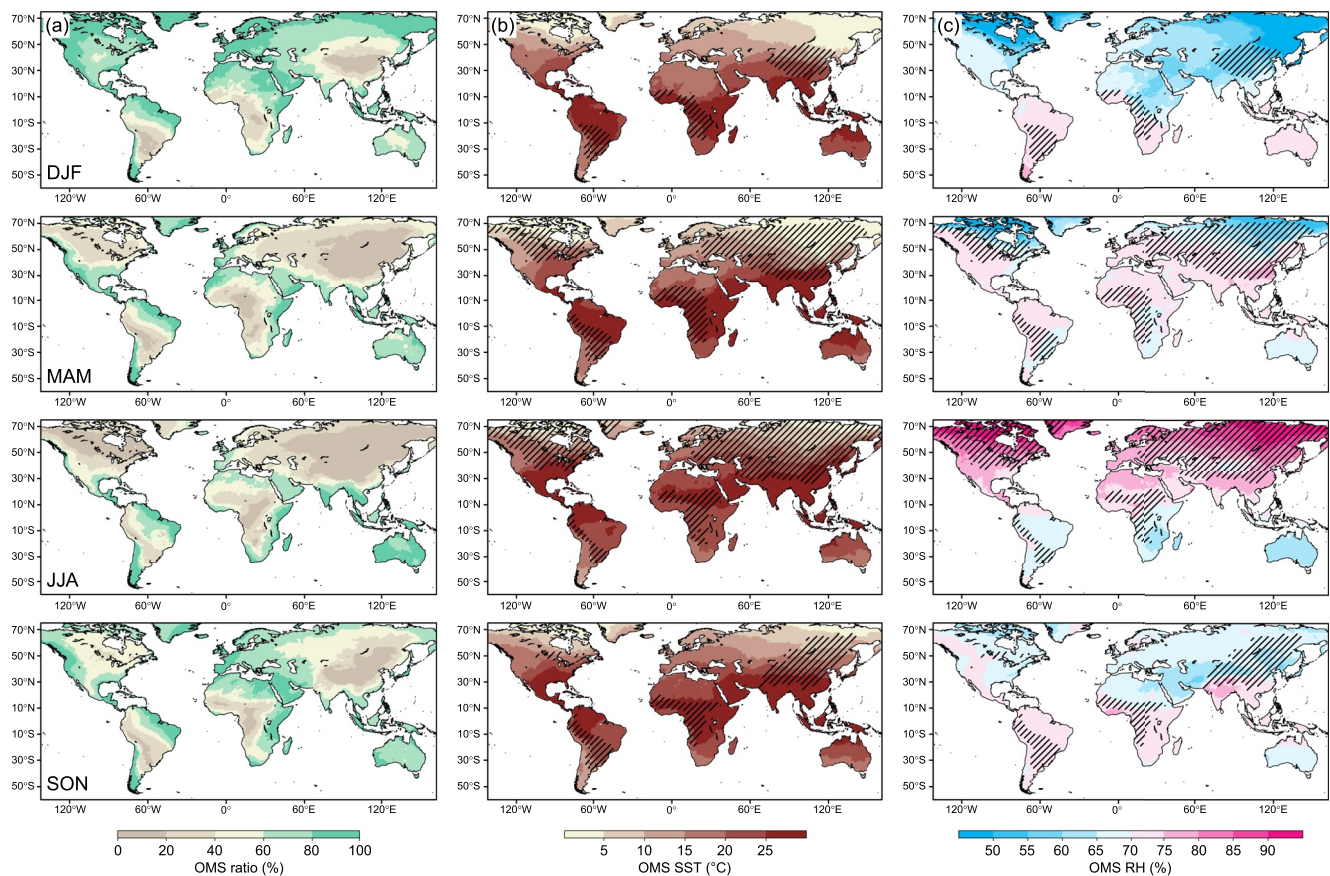


Figure 1. The maps show the (a) oceanic moisture source (OMS) ratio, (b) OMS SST, and (c) OMS RH in different seasons: December–February, March–May, June–August, and September–November. Hatched areas in (b) and (c) indicate where the OMS ratio is <40% as a reference.

2.4. Model and Data Analyses

The relationships between modeled OMS vapor d-excess and observed GNIP precipitation d-excess are examined using the correlation coefficient (Pearson's R) and root-mean-square residual (RMSR). The R^2 measures the proportion of variability in precipitation d-excess explained by OMS dynamics and reflects the strength of OMS fingerprint. The RMSR measures how accurate the modeled OMS vapor d-excess is in representing the absolute values of precipitation d-excess and may reflect the model bias or modification of OMS signals in vapor by subsequent non-OMS processes. I also filter the monthly mean d-excess data set by sample size (the number of data for calculating the monthly mean value), OMS ratio, latitude, and local RH (from ERA5 reanalysis), repeat the above analysis, and investigate how these factors affect the results. For the compiled $\Delta^{17}\text{O}$ data set limited to a few sites, I explore whether precipitation $\Delta^{17}\text{O}$ and d-excess as a pair show a common response to OMS RH but a contrasting sensitivity to OMS SST. By conducting these analyses, I have assumed that multiyear monthly means of isotopic values calculated from models and observations are climatological means and comparable despite spanning over different periods.

3. Results and Discussion

3.1. Global OMS Patterns and Implications for Isotope-Based OMS Tracers

The gridded OMS products are plotted in Figure 1 as seasonal means to show their spatiotemporal patterns. The OMS ratio is low in the interior or downwind areas on continents and has a strong seasonality in the Northern Hemisphere (NH) with very low values (<20%) in spring and summer (Figure 1a). There is a “hysteresis” pattern— \sim 20% higher OMS ratio in autumn than spring in the NH mid-latitudes (Figure S2 in Supporting Information S1)—resulting from the increased importance of terrestrial moisture sources (TMS) in spring related

to continental water storage availability (Humphrey et al., 2016). The OMS SST follows a latitudinal gradient (Figure 1b). The OMS RH is lower in winter and higher in summer and this seasonality is stronger as latitude increases (Figure 1c). There is also a “hysteresis” pattern in OMS SST and RH—the higher OMS SST and lower OMS RH in autumn than spring—because of ocean thermal inertia (Delmotte et al., 2000; Froehlich et al., 2002), except for the OMS RH around the Arctic (Figure S2 in Supporting Information S1). These products quantify the fingerprint of OMS conditions for each land grid cell on monthly timescales based on moisture source diagnostics, representing a major progress from previous studies that did not identify the exact OMS regions (Landais et al., 2012; Leuenberger & Ranjan, 2021; Pfahl & Sodemann, 2014).

However, the OMS conditions here only characterize the fraction of precipitation that directly sources from oceans. The OMS ratio maps show a fundamental and spatiotemporally variable role of TMS (Figure 1a). Therefore, defining isotope-based OMS tracers should be appraised critically and seems at odds with the fact that continents become the major direct moisture sources for precipitation when and where moisture recycling is enhanced. This view has been suggested much earlier, for example, by Armengaud et al. (1998) who found that ~30% of precipitation over the Greenland ice-sheet originates from NH continents and cautioned that it may complicate the interpretation of d-excess as an OMS tracer.

Recently, Zemp et al. (2014) introduced a conceptual framework wherein moisture recycling is suggested to function as a network to distribute oceanic moisture over continents. This framework has implications for understanding the applicability of isotope-based OMS tracers. Even if much precipitation is directly supplied from TMS for a place where and when the OMS ratio is low, the direct TMS still in part originates from oceans and therefore has its own OMS and TMS. These indirect moisture sources are termed as the first cascading OMS and TMS, and so forth (Figure S1 in Supporting Information S1). I show in Figures S3 and S4 in Supporting Information S1 that the first cascading OMS, that is, the oceanic moisture that has undergone one re-evaporative cycle on continents, accounts for up to >30% of precipitation in some areas, and incorporating this part of cascading oceanic moisture only shifts the OMS SST and RH by <2°C and <2%, respectively, in most areas. This at least means that the direct and first cascading OMS are characterized by similar OMS conditions and implies that the low OMS ratio does not invalidate the applicability of isotope-based OMS tracers if the indirect, cascading supply of oceanic moisture propagates similar OMS signals. Still, in some areas such as Eurasian interiors, the direct and first cascading OMS combined only account for a little fraction of precipitation (Figure S3 in Supporting Information S1), meaning that oceanic moisture has to run through multiple re-evaporation cycles to reach inland. There, the water cycle acts like a closed system mostly disconnected from oceans, and consequently, the link between the isotopic composition of local precipitation and OMS conditions is no longer physically meaningful (Wang et al., 2017).

As a reminder, there is a limitation in the applicability of isotope-based OMS tracers due to the role of TMS. The gridded products of OMS conditions derived here inherit this limitation for not accurately characterizing the fraction of precipitation that directly sources from continents and are more robust in places with high OMS ratios.

3.2. The OMS Fingerprint in Precipitation d-excess

Applying the derived OMS products to the globe, monthly mean precipitation d-excess from the GNIP data set is found to correlate with OMS vapor d-excess calculated from SLR and CA models with an R^2 of 0.18 and 0.24 and an RMSR of 3.8‰ and 5.1‰, respectively (Figure 2a). Filtering the data set impacts the results, briefly as follows (Figure 2b): (a) R^2 value increases to 0.27 and 0.41, respectively, when only using those monthly means with a larger sample size to ≥ 15 (Figure 2a); (b) R^2 is slightly higher when filtered for a higher OMS ratio to $\geq 80\%$; (c) R^2 is higher in mid-latitudes but much lower in low-latitudes; (d) R^2 decreases when filtered for a higher local RH to $\geq 80\%$; and (e) RMSR decreases to 3.0‰ and 4.6‰, respectively, when filtered for a larger sample size, but in other cases, it varies within a narrow range, between 3.5‰ and 3.9‰ for the SLR model and between 5.0‰ and 5.4‰ for the CA model.

These statistics provide insights into the fingerprint of OMS conditions in precipitation d-excess. The higher R^2 values from the CA model are strong, independent evidence that both SST and oceanic RH contribute to the spatiotemporal variability in precipitation d-excess on monthly timescales, and the same is true for annual mean d-excess (Figure S5 in Supporting Information S1). This important finding differs from the previous study by Pfahl and Sodemann (2014) who stressed oceanic RH as the single driver of the seasonality in precipitation d-excess. The higher RMSR values from the CA model, due to simulating biased high vapor d-excess values (Figure 2a), may result from inaccuracies in mechanistic model parameters (aerodynamic exponent, diffusivity

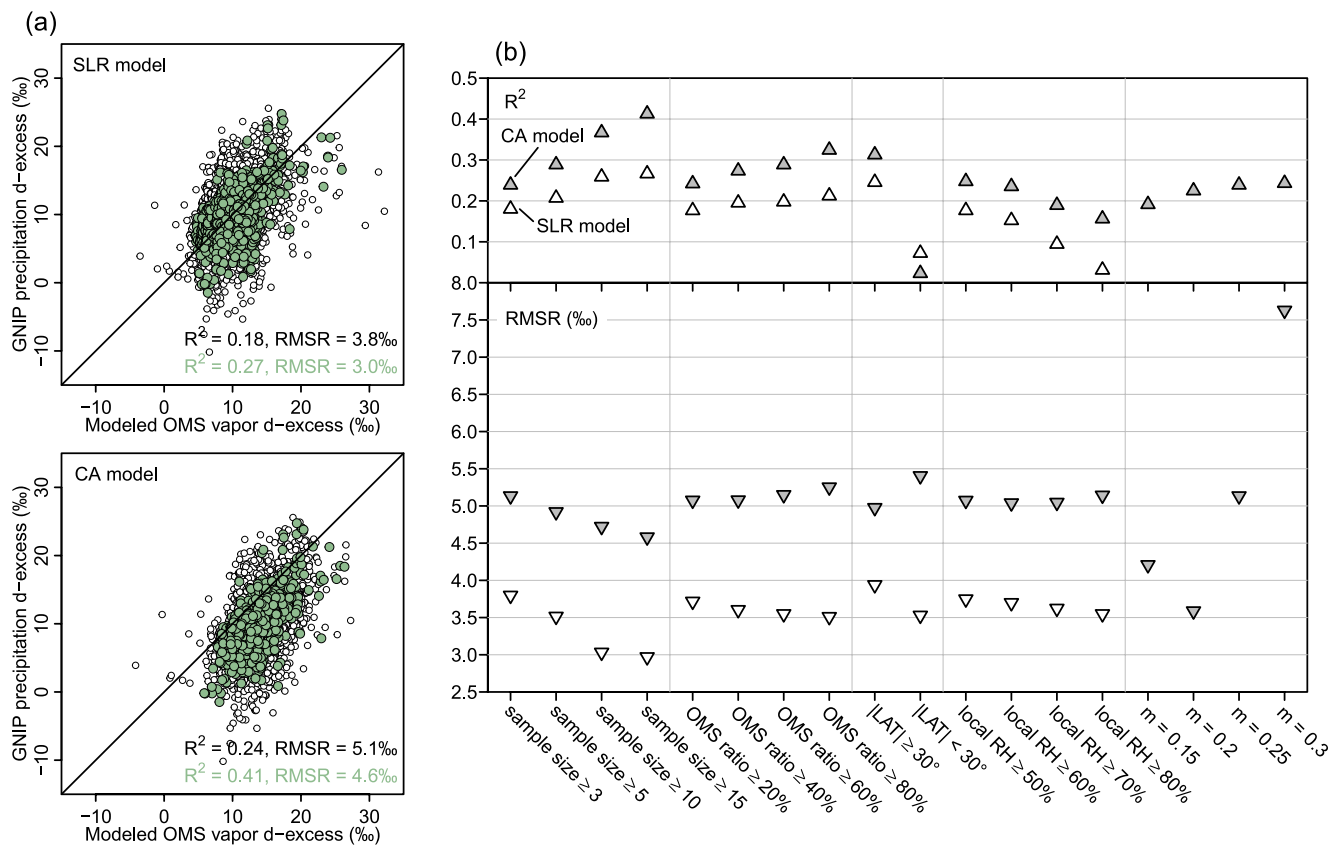


Figure 2. (a) The scatter plots between monthly mean precipitation d-excess from the Global Network of Isotopes in Precipitation (GNIP) data set and oceanic moisture source (OMS) vapor d-excess from two models. Black lines denote the 1:1 relationship for reference. Larger green scatters are those monthly means with a sample size ≥ 15 . (b) Their R^2 and root-mean-square residual (RMSR) values after filtering the data set or using different aerodynamic exponent m values for the closure assumption (CA) model.

ratio, and ocean water d-excess), and do not contradict the higher R^2 the CA model has achieved. For example, weakening the kinetic effect at the ocean-atmosphere interface by setting $m = 0.2$ would decrease RMSR to 3.6‰ (Figure 2b).

Additionally, the analysis of filtered data sets reveals how data set quality, model limitation, and non-OMS processes affect the strength of OMS fingerprint. The stronger OMS fingerprint with a larger sample size indicates that monthly mean d-excess data based on more individual observations and spanning longer periods have higher signal-to-noise ratios as OMS tracers. The stronger OMS fingerprint with a higher OMS ratio is an expected result—again, modeled OMS conditions are more (less) robust for a place with a larger fraction of precipitation directly sourced from oceans (continents). This result also confirms that the cascading supply of oceanic moisture through moisture recycling indeed tends to weaken OMS signals (Xia et al., 2022). The weaker OMS fingerprint in low-latitudes has been previously suggested qualitatively (Xia et al., 2022), and likely results from invariable OMS conditions there (Figures 1b and 1c) and/or the increased importance of non-OMS processes that have modified OMS signals, such as raindrop-vapor interactions in convective systems (Bony et al., 2008; Kurita, 2013). The weaker OMS fingerprint with a higher local RH, however, contradicts the expectation that the local modification of precipitation d-excess by sub-cloud raindrop re-evaporation should have been reduced (Stewart, 1975; Xia et al., 2022), and again likely indicates the increased importance of non-OMS processes. For example, the high local RH often occurs in wet tropics where convection is dominant and affects the isotopic equilibration of raindrops (Bony et al., 2008), or during mid-latitude winter when fractionation related to snow formation in a supersaturated environment affects precipitation d-excess (Jouzel & Merlivat, 1984).

Although the above results might be biased for the over-representation of European sites in the GNIP data set, the consistently low R^2 (at most 0.41) and high RMSR values (at least 3‰) underscore that precipitation d-excess is controlled by the competing influences of OMS and non-OMS processes. As the role of non-OMS processes

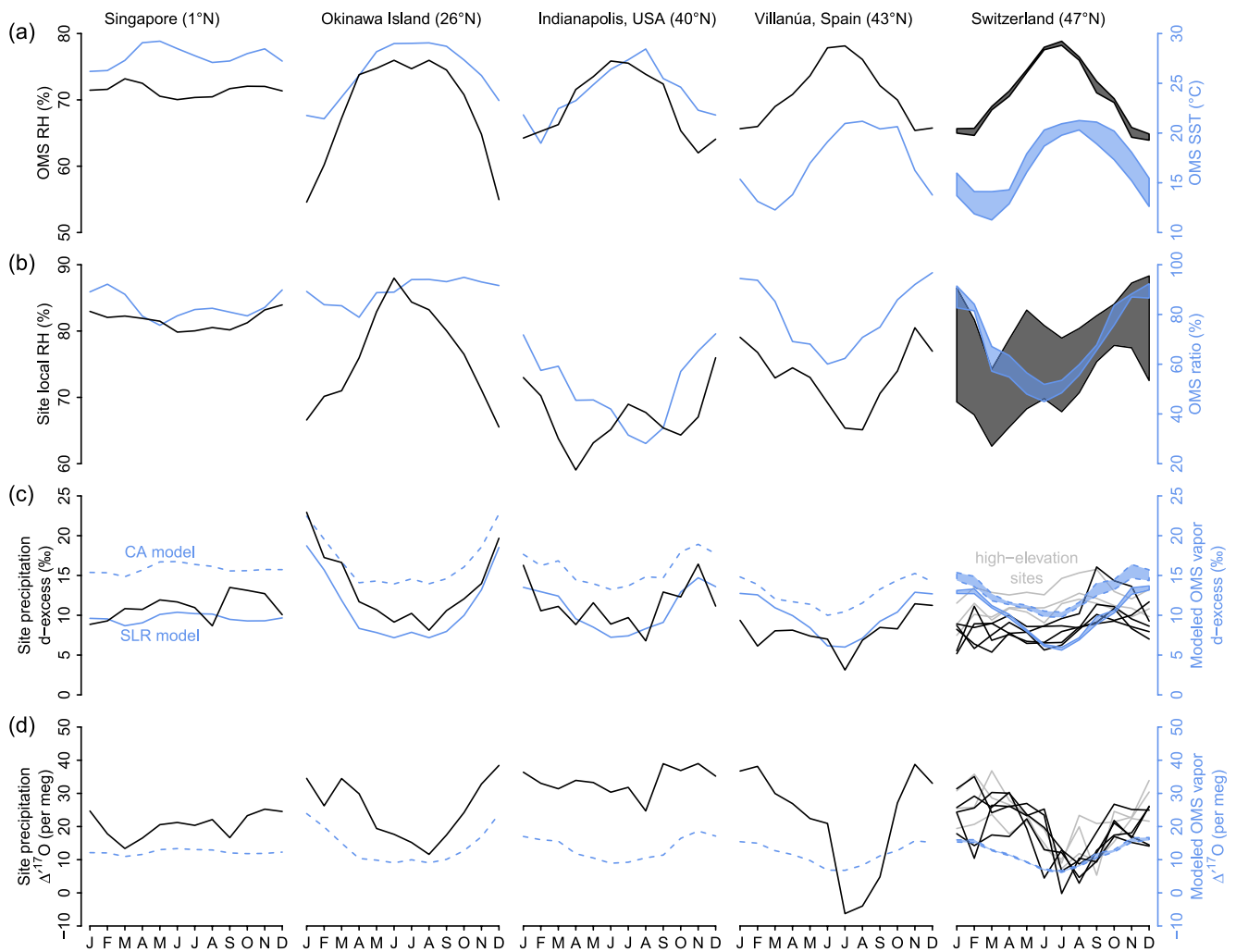


Figure 3. The plots show the 12 monthly means of (a) OMS SST (blue lines) and relative humidity (RH), (b) oceanic moisture source (OMS) ratio (blue lines) and local RH, (c and d) observed precipitation and modeled OMS vapor d-excess (solid and dashed blue lines are from simple linear regression [SLR] and closure assumption [CA] models, respectively) and $\Delta^{17}\text{O}$ (CA model only; SLR-modeled results are almost identical) of four different sites and a region (Switzerland that has eight sites) from the compiled $\Delta^{17}\text{O}$ data set. For the Switzerland sites, values are plotted as ranges except for precipitation isotope data which are plotted individually for each site (three high-elevation sites are marked in gray color).

varies spatiotemporally by multiple mechanisms, future studies should aim to further address their impacts on the use of d-excess and its analog $\Delta^{17}\text{O}$ as OMS tracers at local scales.

3.3. The Contrasting Sensitivity of d-excess and $\Delta^{17}\text{O}$ to OMS SST

For the compiled $\Delta^{17}\text{O}$ data set, the 12 monthly means of d-excess and $\Delta^{17}\text{O}$ in precipitation and their modeled values in OMS vapor, along with OMS conditions and other factors of each site, are plotted in Figure 3 for an overview (precipitation amount is shown in Figure S6 in Supporting Information S1).

The seasonal patterns of modeled OMS vapor d-excess and $\Delta^{17}\text{O}$ appear very similar between SLR (SST driver excluded) and CA (SST driver included) models, despite that the CA model is known to simulate biased high d-excess values (Figures 3c and 3d). OMS SST varies by 7°C–10°C seasonally among these sites (except Singapore), in phase with OMS RH despite having a lag of ~2 months for European sites (Figure 3a). As higher SST increases but higher oceanic RH decreases vapor d-excess (Johnsen et al., 1989; Pfahl & Sodemann, 2014), their in-phase relationships mean that OMS SST only attenuates the magnitude of OMS RH-dominated seasonal changes in vapor d-excess by 2.5–3.5‰ using the known CA model-based sensitivity factor of 0.35‰/°C (Equation 3 in Pfahl & Sodemann, 2014).

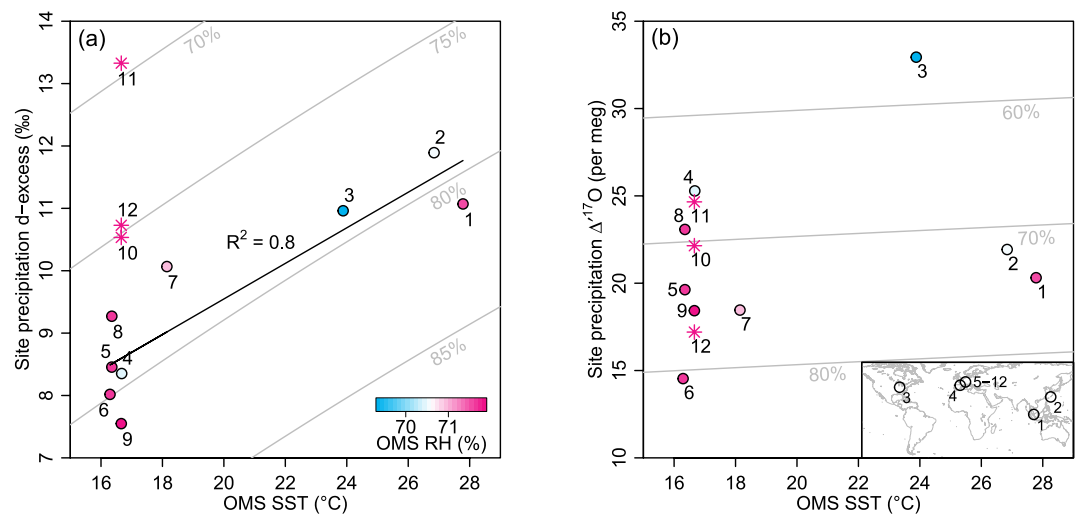


Figure 4. The scatter plots show the independent effect of OMS SST on annual mean precipitation (a) d-excess and (b) $\Delta^{17}\text{O}$ from the compiled $\Delta^{17}\text{O}$ data set. Scatters are individual sites labeled as 1–4 for Singapore, Okinawa Island, Indianapolis, and the Pyrenees, respectively, and 5–12 for Switzerland sites with three high-elevation sites marked as asterisks and excluded in the linear regression. An inset map in (b) shows site locations. Scatters are colored based on OMS RH. Gray lines are contours of CA-modeled vapor d-excess and $\Delta^{17}\text{O}$ (10 per meg added to account for fractionation during condensation; Luz & Barkan, 2010) at different oceanic RH.

Although these sites cover a latitudinal range and are characterized by different climate and moisture source settings, their seasonal patterns of precipitation d-excess and $\Delta^{17}\text{O}$, which are both higher in winter and lower in summer but in Singapore both have a slight seasonality, are correctly captured by modeled OMS vapor d-excess and $\Delta^{17}\text{O}$ and suggest seasonal changes in OMS RH as the common driver, except for the d-excess in Switzerland. However, scatter plots may show negative correlations between precipitation d-excess/ $\Delta^{17}\text{O}$ and OMS SST as an artifact of the in-phase relationship between OMS SST and RH (Figure S7 in Supporting Information S1). Furthermore, as mentioned in Section 3.2, multiple non-OMS processes also contribute to the variability in precipitation d-excess and $\Delta^{17}\text{O}$ and modify their OMS signals.

From above, it is concluded that the contrasting sensitivity between d-excess and $\Delta^{17}\text{O}$ to OMS SST does not stand out at a specific site on monthly/seasonal timescales when their signals in precipitation are dominated by changes in OMS RH and additionally affected by noises related to non-OMS processes.

Nevertheless, the annual mean OMS SST ranges between 16°C and 28°C whereas the annual mean OMS RH varies only between 69% and 72% among these sites (Figure 4). These indicate that any different seasonality in OMS RH tends to be averaged out to a similar value for sites from very different settings and that OMS SST becomes the major environmental gradient under annual mean conditions. Additionally, annual mean precipitation d-excess and $\Delta^{17}\text{O}$ data have an integrated nature and therefore are less affected by short-term noises related to non-OMS processes. A robust, positive correlation ($R^2 = 0.8$, $p < 0.01$) between precipitation d-excess and OMS SST emerges under annual mean conditions after excluding three high-elevation ($>1,000$ m asl) Switzerland sites (Figure 4a). The regression coefficient is $0.29 \pm 0.05\text{‰}/^{\circ}\text{C}$, close to the CA-model predicted value of $0.35\text{‰}/^{\circ}\text{C}$ (Pfahl & Sodemann, 2014), despite the known model bias for simulating higher vapor d-excess at the same oceanic RH (Figure 2a). These high-elevation outliers with distinct higher d-excess compared to nearby low-elevation counterparts might be caused by non-OMS processes at local scales (Leuenberger & Ranjan, 2021), perhaps most importantly by the orographic seeder-feeder mechanism (Liotta et al., 2006). By contrast, there is no clear relationship ($R^2 = 0.11$, $p = 0.34$) between precipitation $\Delta^{17}\text{O}$ and OMS SST (Figure 4b). Therefore, the contrasting sensitivity between d-excess and $\Delta^{17}\text{O}$ to OMS SST initially predicted by the theoretical model is distinguishable from precipitation observations under annual mean conditions from a spatial network of sites.

4. Conclusions

This study disentangles the complex controls of precipitation d-excess and $\Delta^{17}\text{O}$ by quantifying the crucial role of OMS dynamics. I show a dual control of SST and oceanic RH on precipitation d-excess in low- and

mid-latitudes on monthly timescales, together explaining 41% of the spatiotemporal variability, compared to 27% from oceanic RH only (Figure 2a). Accordingly, non-OMS processes, including regional moisture recycling and local condensation or post-condensation modifications, contribute to more than half of the variability in precipitation d-excess, reiterating that d-excess and its analog $\Delta^{17}\text{O}$ are not simple OMS tracers (Xia et al., 2022). Still, I successfully demonstrate that the contrasting sensitivity between d-excess and $\Delta^{17}\text{O}$ to OMS SST is distinguishable from noisy precipitation observational data sets under annual mean conditions across multiple sites. This validation in principle supports the possible use of d-excess and $\Delta^{17}\text{O}$ data as a pair to infer independent OMS SST and RH information (Angert et al., 2004) and underscores the factor of timescales.

Data Availability Statement

The GNIP data set can be accessed through <https://nucleus.iaea.org/wiser>.

The compiled $\Delta^{17}\text{O}$ data set consists of data reported from these studies: Table S1 in He et al. (2021) for Singapore, Table S2 in Uechi and Uemura (2019) for Okinawa Island, <https://doi.org/10.1594/PANGAEA.895300> and Tian and Wang (2019) for Indianapolis in the U.S., Supplementary Table 3 in Giménez et al. (2021) for the Pyrenees in Spain, Figures 4 and 6 in Affolter et al. (2015) for Mormont in Switzerland, and Figures 7–13 in Leuenberger and Ranjan (2021) for other Switzerland sites.

The UTrack atmospheric moisture flow data set can be accessed through <https://doi.org/10.1594/PANGAEA.912710> (Tuinenburg et al., 2020).

The ERA5 reanalysis product (ERA5 monthly averaged data on single levels from 1959 to present) can be accessed through <https://cds.climate.copernicus.eu/> (Hersbach et al., 2020).

The derived products (OMS ratio, OMS SST, and OMS RH for both direct and first cascading OMS) and their source codes are made available on Figshare and can be accessed through <https://doi.org/10.6084/m9.figshare.21936840>.

References

- Affolter, S., Häuselmann, A. D., Fleitmann, D., Häuselmann, P., & Leuenberger, M. (2015). Triple isotope (δD , $\delta^{17}\text{O}$, $\delta^{18}\text{O}$) study on precipitation, drip water, and speleothem fluid inclusions for a Western Central European cave (NW Switzerland). *Quaternary Science Reviews*, 127, 73–89. <https://doi.org/10.1016/j.quascirev.2015.08.030>
- Angert, A., Cappa, C. D., & DePaolo, D. J. (2004). Kinetic ^{17}O effects in the hydrologic cycle: Indirect evidence and implications. *Geochimica et Cosmochimica Acta*, 68(17), 3487–3495. <https://doi.org/10.1016/j.gca.2004.02.010>
- Armengaud, A., Koster, R. D., Jouzel, J., & Ciais, P. (1998). Deuterium excess in Greenland snow: Analysis with simple and complex models. *Journal of Geophysical Research*, 103(D8), 8947–8953. <https://doi.org/10.1029/98JD00274>
- Aron, P. G., Levin, N. E., Beverly, E. J., Huth, T. E., Passey, B. H., Pelletier, E. M., et al. (2021). Triple oxygen isotopes in the water cycle. *Chemical Geology*, 565, 120026. <https://doi.org/10.1016/j.chemgeo.2020.120026>
- Barkan, E., & Luz, B. (2005). High-precision measurements of $^{17}\text{O}/^{16}\text{O}$ and $^{18}\text{O}/^{16}\text{O}$ ratios in H_2O . *Rapid Communications in Mass Spectrometry*, 19(24), 3737–3742. <https://doi.org/10.1002/rcm.2250>
- Barkan, E., & Luz, B. (2007). Diffusivity fractionations of $\text{H}_2^{16}\text{O}/\text{H}_2^{17}\text{O}$ and $\text{H}_2^{16}\text{O}/\text{H}_2^{18}\text{O}$ in air and their implications for isotope hydrology. *Rapid Communications in Mass Spectrometry*, 21(18), 2999–3005. <https://doi.org/10.1002/rcm.3180>
- Bershaw, J., Hansen, D. D., & Schauer, A. J. (2020). Deuterium excess and ^{17}O -excess variability in meteoric water across the Pacific Northwest, USA. *Tellus B: Chemical and Physical Meteorology*, 72(1), 1–17. <https://doi.org/10.1080/16000889.2020.1773722>
- Bony, S., Risi, C., & Vimeux, F. (2008). Influence of convective processes on the isotopic composition ($\delta^{18}\text{O}$ and δD) of precipitation and water vapor in the tropics: 1. Radiative-convective equilibrium and Tropical Ocean-Global Atmosphere-Coupled Ocean-Atmosphere Response Experiment (TOGA-COARE) simulations. *Journal of Geophysical Research*, 113(D19), D19305. <https://doi.org/10.1029/2008JD009942>
- Craig, H., & Gordon, L. I. (1965). Deuterium and oxygen 18 variations in the ocean and the marine atmosphere. In E. Tongiorgi (Ed.), *Proceedings of a Conference on Stable isotopes in oceanographic studies and paleotemperatures* (pp. 9–130). Consiglio nazionale delle Ricerche, Laboratorio di Geologia Nucleare.
- Dansgaard, W. (1964). Stable isotopes in precipitation. *Tellus*, 16(4), 436–468. <https://doi.org/10.3402/tellusa.v16i4.8993>
- Delmotte, M., Masson, V., Jouzel, J., & Morgan, V. I. (2000). A seasonal deuterium excess signal at Law Dome, coastal eastern Antarctica: A southern ocean signature. *Journal of Geophysical Research*, 105(D6), 7187–7197. <https://doi.org/10.1029/1999JD901085>
- Froehlich, K., Gibson, J. J., & Aggarwal, P. K. (2002). *Deuterium excess in precipitation and its climatological significance (IAEA-CSP-13/P)*. International Atomic Energy Agency (IAEA). Retrieved from https://inis.iaea.org/search/search.aspx?orig_q=RN:34017972
- Gat, J. R. (1996). Oxygen and hydrogen isotopes in the hydrologic cycle. *Annual Review of Earth and Planetary Sciences*, 24(1), 225–262. <https://doi.org/10.1146/annurev.earth.24.1.225>
- Gat, J. R., Bowser, C. J., & Kendall, C. (1994). The contribution of evaporation from the Great Lakes to the continental atmosphere: Estimate based on stable isotope data. *Geophysical Research Letters*, 21(7), 557–560. <https://doi.org/10.1029/94GL00069>
- Gat, J. R., & Matsui, E. (1991). Atmospheric water balance in the Amazon basin: An isotopic evapotranspiration model. *Journal of Geophysical Research*, 96(D7), 13179–13188. <https://doi.org/10.1029/91JD00054>
- Giménez, R., Bartolomé, M., Gázquez, F., Iglesias, M., & Moreno, A. (2021). Underlying climate controls in triple oxygen (^{16}O , ^{17}O , ^{18}O) and hydrogen (^1H , ^2H) isotopes composition of rainfall (central Pyrenees). *Frontiers of Earth Science*, 9. <https://doi.org/10.3389/feart.2021.633698>
- He, S., Jackisch, D., Samanta, D., Yi, P. K. Y., Liu, G., Wang, X., & Goodkin, N. F. (2021). Understanding tropical convection through triple oxygen isotopes of precipitation from the Maritime Continent. *Journal of Geophysical Research: Atmospheres*, 126(4), e2020JD033418. <https://doi.org/10.1029/2020JD033418>

Acknowledgments

Z.X. is supported by the NSFC (Grant 42201167). The manuscript benefited from comments by M.J. Winnick and three reviewers.

- Hersbach, H., Bell, B., Berrisford, P., Hirahara, S., Horányi, A., Muñoz-Sabater, J., et al. (2020). The ERA5 global reanalysis. *Quarterly Journal of the Royal Meteorological Society*, 146(730), 1999–2049. <https://doi.org/10.1002/qj.3803>
- Humphrey, V., Gudmundsson, L., & Seneviratne, S. I. (2016). Assessing global water storage variability from GRACE: Trends, seasonal cycle, subseasonal anomalies and extremes. *Surveys in Geophysics*, 37(2), 357–395. <https://doi.org/10.1007/s10712-016-9367-1>
- IAEA/WMO. (2021). Global network of isotopes in precipitation: The GNIP database. Retrieved from <https://nucleus.iaea.org/wiser>
- Johnsen, S. J., Dansgaard, W., & White, J. W. C. (1989). The origin of Arctic precipitation under present and glacial conditions. *Tellus B: Chemical and Physical Meteorology*, 41(4), 452–468. <https://doi.org/10.3402/tellusb.v41i4.15100>
- Jouzel, J., Delaygue, G., Landais, A., Masson-Delmotte, V., Risi, C., & Vimeux, F. (2013). Water isotopes as tools to document oceanic sources of precipitation. *Water Resources Research*, 49(11), 7469–7486. <https://doi.org/10.1002/2013WR013508>
- Jouzel, J., & Merlivat, L. (1984). Deuterium and oxygen 18 in precipitation: Modeling of the isotopic effects during snow formation. *Journal of Geophysical Research*, 89(D7), 11749–11757. <https://doi.org/10.1029/JD089iD07p11749>
- Jouzel, J., Merlivat, L., & Lorius, C. (1982). Deuterium excess in an East Antarctic ice core suggests higher relative humidity at the oceanic surface during the last glacial maximum. *Nature*, 299(5885), 688–691. <https://doi.org/10.1038/299688a0>
- Kurita, N. (2013). Water isotopic variability in response to mesoscale convective system over the tropical ocean. *Journal of Geophysical Research: Atmospheres*, 118(18), 10376–10390. <https://doi.org/10.1002/jgrd.50754>
- Landais, A., Barkan, E., & Luz, B. (2008). Record of $\delta^{18}\text{O}$ and ^{17}O -excess in ice from Vostok Antarctica during the last 150,000 yr. *Geophysical Research Letters*, 35(2), L02709. <https://doi.org/10.1029/2007GL032096>
- Landais, A., Steen-Larsen, H. C., Guillevic, M., Masson-Delmotte, V., Vinther, B., & Winkler, R. (2012). Triple isotopic composition of oxygen in surface snow and water vapor at NEEM (Greenland). *Geochimica et Cosmochimica Acta*, 77, 304–316. <https://doi.org/10.1016/j.gca.2011.11.022>
- Leuenberger, M. C., & Ranjan, S. (2021). Disentangle kinetic from equilibrium fractionation using primary ($\delta^{17}\text{O}$, $\delta^{18}\text{O}$, δD) and secondary ($\Delta^{17}\text{O}$, d_{ex}) stable isotope parameters on samples from the Swiss precipitation network. *Frontiers of Earth Science*, 9. <https://doi.org/10.3389/feart.2021.598061>
- Li, S., Levin, N. E., & Chesson, L. A. (2015). Continental scale variation in ^{17}O -excess of meteoric waters in the United States. *Geochimica et Cosmochimica Acta*, 164, 110–126. <https://doi.org/10.1016/j.gca.2015.04.047>
- Liotta, M., Favara, R., & Valenza, M. (2006). Isotopic composition of the precipitations in the central Mediterranean: Origin marks and orographic precipitation effects. *Journal of Geophysical Research*, 111(D19), D19302. <https://doi.org/10.1029/2005JD006818>
- Luz, B., & Barkan, E. (2010). Variations of $^{17}\text{O}/^{16}\text{O}$ and $^{18}\text{O}/^{16}\text{O}$ in meteoric waters. *Geochimica et Cosmochimica Acta*, 74(22), 6276–6286. <https://doi.org/10.1016/j.gca.2010.08.016>
- Majoube, M. (1971). Fractionnement en oxygène 18 et en deutérium entre l'eau et sa vapeur. *Journal de Chimie Physique*, 68, 1423–1436. <https://doi.org/10.1051/jcp/1971681423>
- Merlivat, L. (1978). Molecular diffusivities of H_2^{16}O , HD^{16}O , and H_2^{18}O in gases. *The Journal of Chemical Physics*, 69(6), 2864–2871. <https://doi.org/10.1063/1.436884>
- Merlivat, L., & Jouzel, J. (1979). Global climatic interpretation of the deuterium-oxygen 18 relationship for precipitation. *Journal of Geophysical Research*, 84(C8), 5029–5033. <https://doi.org/10.1029/JC084iC08p05029>
- Pang, Z., Kong, Y., Froehlich, K., Huang, T., Yuan, L., Li, Z., & Wang, F. (2011). Processes affecting isotopes in precipitation of an arid region. *Tellus B: Chemical and Physical Meteorology*, 63(3), 352–359. <https://doi.org/10.1111/j.1600-0889.2011.00532.x>
- Pfahel, S., & Sodemann, H. (2014). What controls deuterium excess in global precipitation? *Climate of the Past*, 10(2), 771–781. <https://doi.org/10.5194/cp-10-771-2014>
- Pfahel, S., & Wernli, H. (2009). Lagrangian simulations of stable isotopes in water vapor: An evaluation of nonequilibrium fractionation in the Craig-Gordon model. *Journal of Geophysical Research*, 114(D20), D20108. <https://doi.org/10.1029/2009JD012054>
- Putman, A. L., Fiorella, R. P., Bowen, G. J., & Cai, Z. (2019). A global perspective on Local Meteoric Water Lines: Meta-analytic insight into fundamental controls and practical constraints. *Water Resources Research*, 55(8), 6896–6910. <https://doi.org/10.1029/2019WR025181>
- Risi, C., Landais, A., Winkler, R., & Vimeux, F. (2013). Can we determine what controls the spatio-temporal distribution of d-excess and ^{17}O -excess in precipitation using the LMDZ general circulation model? *Climate of the Past*, 9(5), 2173–2193. <https://doi.org/10.5194/cp-9-2173-2013>
- Rozanski, K. (1985). Deuterium and oxygen-18 in European groundwaters—Links to atmospheric circulation in the past. *Chemical Geology*, 52(3), 349–363. [https://doi.org/10.1016/0168-9622\(85\)90045-4](https://doi.org/10.1016/0168-9622(85)90045-4)
- Schoenemann, S. W., Steig, E. J., Ding, Q., Markle, B. R., & Schauer, A. J. (2014). Triple water-isotopologue record from WAIS Divide, Antarctica: Controls on glacial-interglacial changes in $^{17}\text{O}_{\text{excess}}$ of precipitation. *Journal of Geophysical Research: Atmospheres*, 119(14), 8741–8763. <https://doi.org/10.1002/2014JD021770>
- Stewart, M. K. (1975). Stable isotope fractionation due to evaporation and isotopic exchange of falling waterdrops: Applications to atmospheric processes and evaporation of lakes. *Journal of Geophysical Research*, 80(9), 1133–1146. <https://doi.org/10.1029/JC080i009p01133>
- Taupin, J.-D., Coudrain-Ribstein, A., Gallaire, R., Zuppi, G. M., & Filly, A. (2000). Rainfall characteristics ($\delta^{18}\text{O}$, $\delta^2\text{H}$, ΔT , and ΔH_i) in western Africa: Regional scale and influence of irrigated areas. *Journal of Geophysical Research*, 105(D9), 11911–11924. <https://doi.org/10.1029/1999JD901032>
- Tian, C., & Wang, L. (2019). Stable isotope variations of daily precipitation from 2014–2018 in the central United States. *Scientific Data*, 6(1), 190018. <https://doi.org/10.1038/sdata.2019.18>
- Tuinenburg, O. A., & Staal, A. (2020). Tracking the global flows of atmospheric moisture and associated uncertainties. *Hydrology and Earth System Sciences*, 24(5), 2419–2435. <https://doi.org/10.5194/hess-24-2419-2020>
- Tuinenburg, O. A., Theeuwens, J. J. E., & Staal, A. (2020). High-resolution global atmospheric moisture connections from evaporation to precipitation. *Earth System Science Data*, 12(4), 3177–3188. <https://doi.org/10.5194/essd-12-3177-2020>
- Uechi, Y., & Uemura, R. (2019). Dominant influence of the humidity in the moisture source region on the ^{17}O -excess in precipitation on a subtropical island. *Earth and Planetary Science Letters*, 513, 20–28. <https://doi.org/10.1016/j.epsl.2019.02.012>
- Uemura, R., Barkan, E., Abe, O., & Luz, B. (2010). Triple isotope composition of oxygen in atmospheric water vapor. *Geophysical Research Letters*, 37(4), L04402. <https://doi.org/10.1029/2009GL041960>
- Vimeux, F., Masson, V., Jouzel, J., Stievenard, M., & Petit, J. R. (1999). Glacial-interglacial changes in ocean surface conditions in the Southern Hemisphere. *Nature*, 398(6726), 410–413. <https://doi.org/10.1038/18860>

- Wang, S., Zhang, M., Crawford, J., Hughes, C. E., Du, M., & Liu, X. (2017). The effect of moisture source and synoptic conditions on precipitation isotopes in arid central Asia. *Journal of Geophysical Research: Atmospheres*, *122*(5), 2667–2682. <https://doi.org/10.1002/2015JD024626>
- Xia, Z., Welker, J. M., & Winnick, M. J. (2022). The seasonality of deuterium excess in non-polar precipitation. *Global Biogeochemical Cycles*, *36*(10), e2021GB007245. <https://doi.org/10.1029/2021GB007245>
- Zemp, D. C., Schleussner, C. F., Barbosa, H. M. J., van der Ent, R. J., Donges, J. F., Heinke, J., et al. (2014). On the importance of cascading moisture recycling in South America. *Atmospheric Chemistry and Physics*, *14*(23), 13337–13359. <https://doi.org/10.5194/acp-14-13337-2014>